UCRL-JC-119863
PREPRINT
CONF-950778--2

Remote Measurement of Ground Source Emissivity

John R. Henderson

This paper was prepared for submittal to the
International Symposium on Optical Science, Engineering and Instrumentation
San Diego, CA
July 9-14, 1995

July 1995

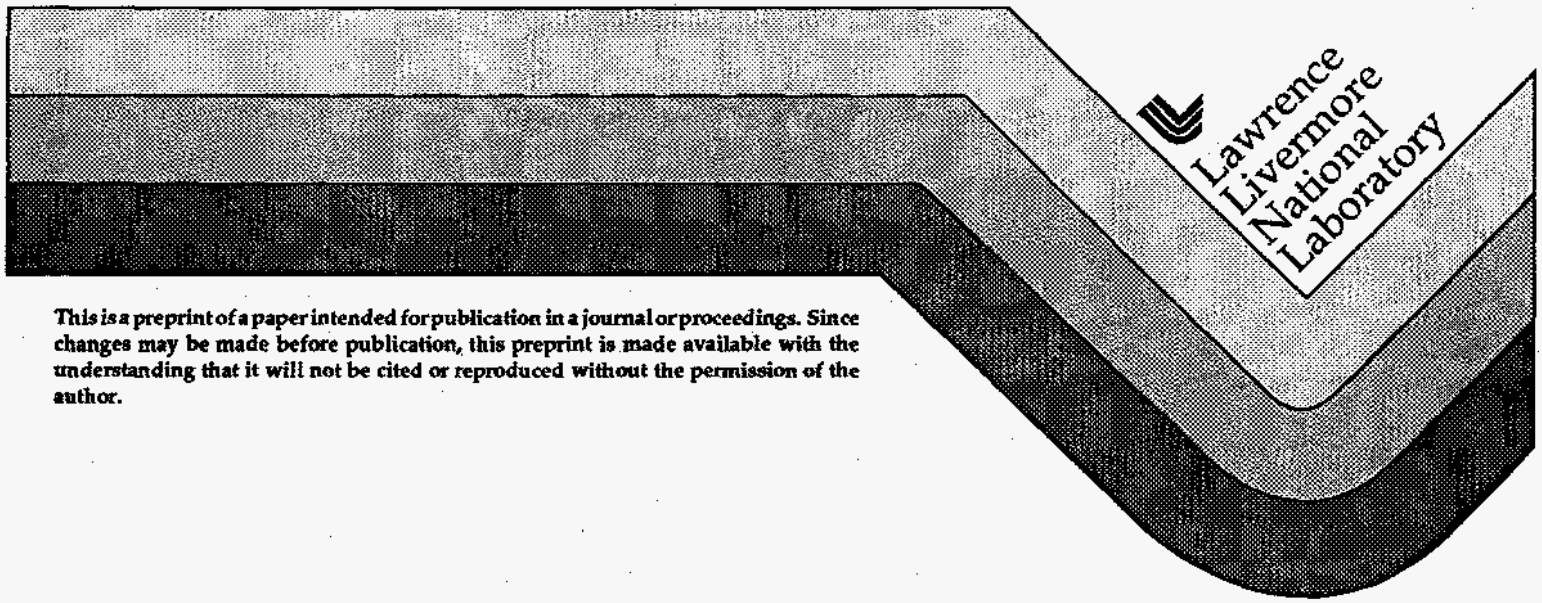

This is a preprint of a paper intended for publication in a journal or proceedings. Since changes may be made before publication, this preprint is made available with the understanding that it will not be cited or reproduced without the permission of the author.

DISTRIBUTION OF THIS DOCUMENT IS UNLIMITED

MASTER

DISCLAIMER

This report was prepared as an account of work sponsored by an agency of the United States Government. Neither the United States Government nor any agency thereof, nor any of their employees, make any warranty, express or implied, or assumes any legal liability or responsibility for the accuracy, completeness, or usefulness of any information, apparatus, product, or process disclosed, or represents that its use would not infringe privately owned rights. Reference herein to any specific commercial product, process, or service by trade name, trademark, manufacturer, or otherwise does not necessarily constitute or imply its endorsement, recommendation, or favoring by the United States Government or any agency thereof. The views and opinions of authors expressed herein do not necessarily state or reflect those of the United States Government or any agency thereof.

DISCLAIMER

Portions of this document may be illegible in electronic image products. Images are produced from the best available original document.

surfaces, Macleod[5] obtained 0.3K for an airborne platform, and Byrnes and Schott[2] measured rms errors of 1.0K to 6.6K at altitudes of 1000 feet to 6000 feet, respectively. Simulations by Cogan[6] support the magnitude and linear scaling with altitude observed.

The two-angle techniques mentioned above all use a band averaged transmission which creates a systematic underestimate of the transmission off-nadir. More generally, for a given waveband there are three parameters that determine the measured emission: the source emission, the atmospheric transmission, and the atmospheric emission. Equivalently, one can use an effective atmospheric temperature and emissivity (determined from the transmission). The fundamental difficulty with two-angle techniques is that the problem is underconstrained. A minimum of three measurements are needed to solve for this simple model of atmospheric effects, but only two measurements are made. For low altitudes, the atmospheric emission is comparatively small. Two angles techniques either ignore the atmospheric emission, or assume a reasonable atmospheric temperature and emissivity. The errors from the latter are typically small. For high altitude platforms or conditions of poor visibility, the atmospheric emission must be treated accurately, and two-angle techniques are inadequate.

Previous work[7,8] has shown that the multi-angle technique overcomes these problems. This allows remote measurements of source thermal emission that are accurate, even under conditions of poor atmospheric transmission.

The remaining problem of determining the source emissivity and reflectivity is investigated here. In section 2 the model and necessary equations are developed. Section 3 describes the generation of the synthetic data used in these analyses. The results of fitting to these data are then described in section 4, particularly in terms of the source emissivity and reflectivity. Section 5 gives the conclusions and some discussion of the implications of this work.

2. SOURCE AND ATMOSPHERE MODELS

Details and justification of the models are given in references 7 and 8. In general, all the parameters are a function of wavelength, except for the source temperature. The wavelength dependence will be suppressed in the nomenclature here. The parameters of interest are described in Table 1 for convenience.

The measured signal at a remote detector is

$$L_d = \tau * L_s + L_a \,, \tag{1}$$

Remote measurement of ground source emissivity

John R. Henderson

Physics and Space Technology, MS L-043
Lawrence Livermore National Laboratory
Livermore, California 94550

ABSTRACT

The remote measurement of the emissivity of ground materials is of tremendous value in their identification and mapping. Traditional techniques use reflected solar radiation for this measurement for wavelengths shorter than 5 μm. With the development of new techniques, the 10 μm atmospheric transmission window might also be used for this purpose. Previous work using the multi-angle data acquisition technique demonstrated its utility to determine source thermal emission. Here we find the multi-angle technique can be used to determine the source specular reflectivity to ~0.05 if there is very good system performance (NETD ≈ 0.01 K).

Keywords: multi-angle, emissivity, resource mapping

1. INTRODUCTION

The goal of this work is to develop techniques to allow the accurate determination of the temperature of ground sources using remote measurements of the sources' thermal emission. Conversion of thermal emission into an accurate source temperature depends critically on knowledge of the source emissivity and reflectivity. Emissivity measurements are difficult and techniques for remote determination of source emissivity are only recently being developed (reference 1 and references within). The remote determination of source emissivity is intrinsically interesting. The variation of emissivity with wavelength gives a fairly unique signature that can be used for materials identification. The ability to use remote sensing for resource mapping is of great value in the fields of agriculture, forestry, and mineral exploration.

A multi-altitude technique[2] can accurately measure the source thermal emission, but is not suitable for satellites or other high altitude platforms. Techniques using multiple (specifically two) viewing angles to enhance remote measurements were proposed[3] at least as early as 1967. The multi-angle technique exploits the variation of the transmission and the emission of the atmosphere with the variation of the depth of the atmospheric column. As the viewing angle deviates from the nadir, the column depth increases, the atmospheric emission increases, and the flux seen at a remote sensor decreases for a ground source warmer than the atmosphere. A wide range of accuracies are reported using the technique: Chedin *et al* [4] obtain rms deviations of 1K to 2K simulating satellite observations of sea

Table 1. Parameters of interest.

B_a	Atmosphere black body thermal emission, transmissive region
B_o	Atmosphere black body thermal emission, opaque region
B_s	Source black body thermal emission
f1	Transmissive fraction of waveband
l	Relative atmospheric column depth (l = 1 at nadir)
L_s	Source thermal emission
L_a	Atmospheric thermal emission
L_d	Detected thermal emission
R_s	Source specular reflectivity
R_d	Source diffuse reflectivity
T_a	Effective atmosphere temperature, transmissive region
T_o	Effective atmosphere temperature, opaque region
T_s	Source temperature
ε_A	Sky averaged atmosphere emissivity
ε_a	Path specific atmosphere emissivity
ε_s	Source emissivity
τ	Atmospheric transmission
τ_o	Atmospheric transmission at nadir
τ_1	Transmission at nadir of transmissive part of waveband

where L_d is the measured emission, τ is the atmospheric transmission, L_s is the source emission, and L_a is the atmospheric emission.

The standard development of multi-angle techniques uses a band-averaged transmission, τ. Taking θ to be the angle from nadir, the transmission as a function of angle is given by

$$\tau = \tau_o^{1/\cos\theta} = \tau_o^{\sec\theta} = \tau_o^{l}, \tag{2}$$

where τ_o is the transmission at nadir and l is the *relative* depth of the atmosphere. For a non-reflective material (the atmosphere) the emissivity and transmissivity are related by

$$\tau = 1 - \varepsilon\,. \tag{3}$$

The atmospheric emission, L_a, is given by

$$L_a = \varepsilon_a * B_\nu(T_a, \lambda_1, \lambda_2)\,, \tag{4}$$

where $B_\nu(T_a, \lambda_1,\lambda_2)$ is the black body emission for a source at temperature T_a over the waveband from λ_1 to λ_2. Hereafter, the explicit wavelength dependence will be suppressed and we will use the shorthand $B_a = B_\nu(T_a, \lambda_1,\lambda_2)$, and $B_s = B_\nu(T_s, \lambda_1,\lambda_2)$ for the atmosphere and source black body emission.

The source is assumed to have an emissivity ε_s, specular reflectivity R_s, and diffuse reflectivity R_d, which are related by

$$1 = \varepsilon_s + R_s + R_d \,. \tag{5}$$

The source emission is then,

$$L_s = \varepsilon_s * B_s + R_d * \varepsilon_A * B_a + R_s * \varepsilon_a * B_a \,, \tag{6}$$

where ε_A is the angular average of the sky emissivity, and it has been assumed that the downwelled sky emission is equal to the upwelled sky emission. ε_A is a function of τ_o and the scene geometry (see Appendix A). ε_a is the path-dependent sky emission and will vary with l (see equations 3 and 7).

The first order model is a two parameter model that divides the band into a transmissive and an opaque region. The parameters are the transmissive fraction of the band, f_1, and its transmission, τ_1. The opaque portion has a transmission of zero and accounts for a fraction $(1 - f_1)$ of the band. The depth-dependent transmission, $\tau(l)$, is now given by

$$\tau(l) = f_1 * (\tau_1{}^l) \,. \tag{7}$$

By definition

$$\tau(l = 1) = f_1 * \tau_1 = \tau_o \,. \tag{8}$$

The atmospheric emission is now given by

$$L_a = f_1 * (1 - \tau_1{}^l) * B_a + (1 - f_1) * B_o, \tag{9}$$

where B_o is the emission for a black body at the temperature, T_o, of the opaque layer. (By definition, the opaque layer has an emissivity on one.)

The flux seen at a detector can be derived using equations 1, 3, 6, 7, and 9. The result is

$$L_d(l) = A + B * \tau_1{}^l + C * \tau_1{}^{2l} \,, \tag{10}$$

where

$$A = f_1 * B_a + (1 - f_1) * B_o \ , \tag{11}$$

$$B = \varepsilon_s * B_s + R_d * \varepsilon_A * B_a + R_s * (1 - f_1) * B_o + R_s * f_1 * B_a - B_a \ , \tag{12}$$

$$C = - f_1^2 * R_s * B_a \ . \tag{13}$$

Here, there are nine parameters of interest, B_s, ε_s, R_d, R_s, B_a, B_o, ε_A, f_1, and τ_1. There are seven constraints: the fit value for τ_1 from equation 10; the fit values for A, B, and C from equation 10 along with equations 11, 12 and 13; equation 5; the relation between ε_A and τ_o; and the determination of f_1 from measurements or simulations[7,8]. The problem is underconstrained for any single waveband. Since T_s is independent of wavelength, T_a and T_o nearly so (depending on the average optical depth in the band), and there are generally some constraints on the ground properties, such as slow variation of ε_s with wavelength, the problem is likely to be constrained for multiple wavebands.

3. SYNTHETIC DATA AND FITTING

The ability to retrieve source parameters was investigated using synthetic data. The data was generated assuming a 15 look pass at uniform velocity and altitude with $l = 1$ to $l = 2.5$. Values for B_a and B_o were taken to be 273 K, and 260 K. Source temperatures of 278 K and 300 K were used. Low (f_1, τ_1 = 0.6, 0.4) and high (f_1, τ_1 = 1.0, 0.9) transmission regimes were used. ε_A was determined using the relation in Appendix A. Two material types were investigated: a "typical" material with $\varepsilon_s = 0.80$, $R_d = 0.15$, and $R_s = 0.05$; and a weathered metallic surface with $\varepsilon_s = 0.15$, $R_d = 0.45$, and $R_s = 0.40$.

A noise-free set of "pure" measurements were generated using equations 10 to 13. Fluxes were normalized to the value at 273 K. Ten data sets were generated from the pure set by adding random noise with a Gaussian NETD of 0.01, 0.05, or 0.20 K. Figure 1a shows some of the data for a "typical" material. The curve falls as the source is viewed through a longer column of atmosphere since the atmosphere is colder than the source. In contrast, Figure 1b shows some data for a metallic source. Here, the observed emission increases with increasing column depth because the effective temperature of the source is much colder than the atmosphere. Since the atmosphere is not opaque, the effective source temperature is a combination of the true source temperature, the temperature of the sky, and the temperature of space (effectively zero). With increasing atmospheric column depth, the path becomes more opaque and the emission approaches that expected for the effective atmosphere temperature.

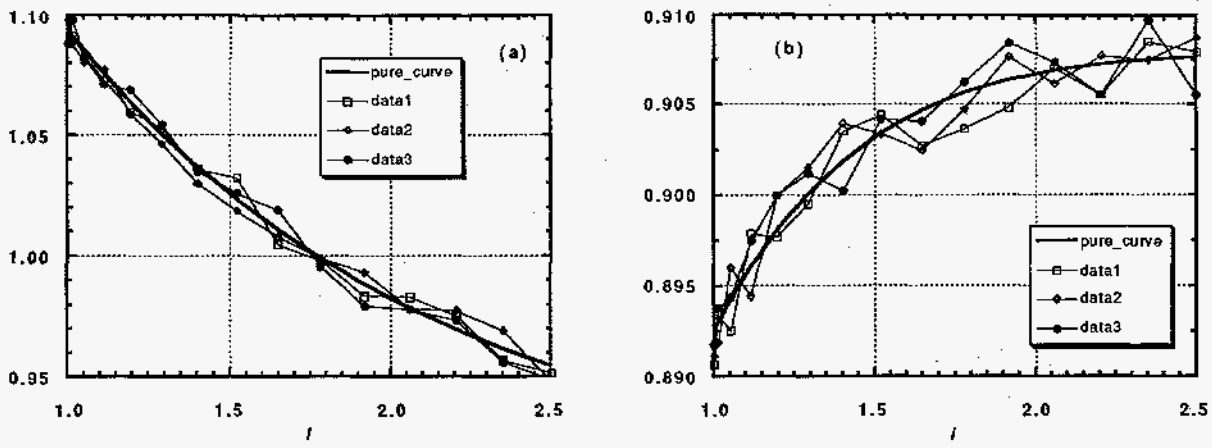

Figure 1. (a) Data from low atmospheric transmission, 300K "typical" material source with NETD = 0.2 K. (b) Data from low atmospheric transmission, 300K "metallic" material source with NETD = 0.05 K.

4. "DATA" INVERSION AND ANALYSIS

A non-linear least-squares fit was done to each of the ten data sets using the form of equation 10. The average and standard deviation of each fit parameter was compared to the expected values to ensure consistency. Table 2 shows one set of data and a comparison to the true values used to generate the data.

There are practical difficulties with fitting to equation 10. For regimes where there is little curvature in the data (high transmission, or atmosphere and source close in temperature), the data are nearly linear and the B and C parameters are highly correlated with large uncertainties. This was discussed previously[8]. The only way to avoid this problem is to use data with very small noise so the curvature is detectable. For the range of conditions investigated, an NETD of 0.2 K was always too large for sensible data inversion. NETD = 0.05 was reasonable for the best conditions, and NETD = 0.01K was even too large for the most demanding conditions. NETD = 0.01K was taken as a practical limit, and lower values were not investigated.

There is also a systematic problem in that there are many local minima for the chi-square function in parameter space. Great care has to be taken to choose the starting values for the fit parameters in order to find the global minimum. The procedure used here, was to start with generic values of the fit parameters. If the evaluated chi-square was more than an order of magnitude greater than the expected value, the fit was restarted with values

Table 2. Results of 10 fits to low atmospheric transmission, cold source with NETD = 0.01K.

trial #	A	B	C	τ_1
1	0.9079	0.5256	-0.1044	0.3831
2	0.9127	0.4399	0.0541	0.3936
3	0.9222	0.6572	-0.3429	0.3094
4	0.9112	0.5138	-0.0751	0.3755
5	0.9002	0.3564	0.1464	0.4594
6	0.9167	0.6862	-0.4075	0.3171
7	0.9177	0.6231	-0.2736	0.3276
8	0.8861	0.1966	0.3281	0.5617
9	0.9036	0.4912	-0.0580	0.4052
10	0.9174	0.6521	-0.3422	0.3240
avg.	0.90957	0.51421	-0.10751	0.38566
sigma	0.01068	0.15379	0.23850	0.07794
true	0.90700	0.47400	-0.01800	0.40000
error	0.00257	0.04021	-0.08951	-0.01434

closer to the expected ones. Sometimes, additional searching had to be done to find a set of starting values that gave an acceptable chi-square. There are local minima within the global chi-square valley that are reached depending on the initial conditions. The differences in the fit values between these near-global minima can be comparable to the variation in the fit values. Here the statistical and systematic errors are treated separately to indicate when this distinction is important.

The specular reflectivity is the most direct material parameter to obtain. From equation 11,

$$B_a = \frac{A - B_o}{f_1} + B_o \ . \tag{14}$$

Equations 13 and 14 can be combined to give

$$R_s = -C \ / \ [f_1*(A - B_o) + f_1^2*B_o] \ . \tag{15}$$

Standard error propagation techniques were used with equation 15 to determine the statistical error in R_s. Parameters A and C are correlated so it is not quite accurate to assume their uncertainties are independent. The errors from this assumption are small since the contribution to the uncertainty in R_s from the determination of parameter C is always significantly larger than that from parameter A. The uncertainty in f_1 was taken to

Table 3. Comparison of R_S determined from synthetic data under a variety of conditions. For full description of conditions, see section 3. Statistical uncertainties are given first. Systematic uncertainties are given last.

	"metallic" source Rs = 0.4 NETD = 0.01 K		"typical" source Rs = 0.05 NETD = 0.05 K
	Ts = 278K	Ts = 300K	Ts = 300K
$f_1, \tau_1 = 0.6, 0.4$	$0.408 \pm 0.056 \pm 0.009$	$0.528 \pm 0.089 \pm 0.566$	$0.297 \pm 0.660 \pm 0.015$
$f_1, \tau_1 = 1.0, 0.9$	$0.426 \pm 0.028 \pm 0.040$	$0.397 \pm 0.030 \pm 0.081$	$0.086 \pm 0.006 \pm 0.047$

be 0.0002 when $f_1 = 1.0$ and 0.03 when $f_1 = 0.6$. These values are determined from MODTRAN runs and assuming the atmospheric water vapor content can be determined to an accuracy of 30%. The uncertainty in B_0 was taken to be 2 K. The results of the determination of R_S are given in Table 3.

For the given conditions, it appears possible to do accurate retrieval of R_S for all the conditions explored if the NETD = 0.01 K. (The R_S uncertainties for the "typical" source need to be lowered by a factor of 5 to compare with those for the "metallic" source because of the different NETD's.) This conclusion is tempered by the fact that very low NETD's were used to ensure reasonable data inversions. It is worth noting that the multi-angle technique does provide the capability to make measurements under conditions of poor transmission nearly as well as under conditions of high transmission. The specific value of R_S seems to have little effect on the ability to retrieve R_S.

For a single waveband, it is not possible to determine the source emissivity. Using equation 5, equation 12 becomes

$$B = \varepsilon_S*(B_S - \varepsilon_A*B_a) + R_S*[(1 - f_1)*B_0 + (f_1 - \varepsilon_A)*B_a], \quad (16)$$

where the only unknowns are ε_S and B_S, ε_A being estimable using f_1, τ_1 and equation A6. While B_S in one waveband determines it in all others, the same cannot be said for the emissivity. Each additional waveband used will add another parameter, leaving the problem undefined. Any constraining relations on the emissivity make the problem soluble, and potentially overdetermined. An example of this would be for data acquired at very high resolution. Since solid materials exhibit emissivity signatures with a characteristic width of a few wavenumbers, resolution higher than this would allow the constraint that the emissivity in one bin is nearly equal to that of its neighbors.

5. SUMMARY AND CONCLUSIONS

It has been shown that it is possible to do accurate retrieval of source specular reflectivity, but only under the extreme condition of very low noise (NETD < 0.05 K). For less demanding conditions, it may not be possible to perform the data inversion needed to obtain the material parameters.

The multi-angle technique is not sufficient to determine the source emissivity and temperature for a single waveband. It should be possible to do so with a sufficiently high spectral resolution system. For a low spectral resolution system, such constraints may not be available due to the essentially independent emissivity in each waveband. However, it should still be possible to do positive materials identification using the spectral signature of the specular reflectivity. A database of specular reflectivity signatures would have to be analyzed to evaluate the uniqueness of such signatures. Assuming the signature was sufficiently unique, the source material and emissivity would be identified and a temperature determination could be made.

Here, the determination of parameters of interest was performed assuming uncorrelated variables. Some increase in inversion capability is obtainable by fitting to a more complicated fitting function containing all the parameters of interest, along with any cross-waveband constraints. This is a significantly larger problem than considered here. This work can be taken as a guide to evaluate when the larger effort would become worthwhile.

6. ACKNOWLEDGMENTS

This work was performed under the auspices of the U.S. Department of Energy by Lawrence Livermore National Laboratory under contract No. W-7405-Eng-48.

7. REFERENCES

1. Sylvia Keirse and Eon O Mongain, "Top of atmosphere radiance estimates with assessment of data quality," *SPIE Proceedings 2471-09*, April 1995 (in press).

2. A. E. Byrnes and J. R. Schott, "Correction of thermal imagery for atmospheric effects using aircraft measurement and atmospheric modeling techniques," *Appl. Opt.*, **25**, pp. 2563 - 2570, August 1986.

3. P. M. Saunders, "Aerial Measurements of Sea Surface Temperature in the Infrared," *J. Geophys. Res.*, **72**, pp. 4109 - 4117, 1967.

4. A. Chedin, N. A. Scott, and A. Berroir, "A Single Channel Double-Viewing Angle Method for Sea Surface Temperature Determination from Coincident METEOSAT and TIROS-N Radiometric Measurements," *J. Appl Meterol.*, **15**, p. 173, 1976.

5. I. D. Macleod, "An Airborne Thermal Remote Sensing Technique," M.S. Thesis, Rochester Institute of Technology, Rochester, NY, 1983.

6. J. L. Cogan, "Passive remote sensing of slant path transmittance," *Appl. Opt.*, **27**, pp 3280-3289, August 1988.

7. J. R. Henderson, "Remote Measurement of ground Temperature and Emissivity," *SPIE Proceedings 2269*, pp. 610-521, July 1994.

8. J. R. Henderson, "Multi-angle technique for measurement of ground source emission," *SPIE Proceedings 2471-51*, April 1995 (in press).

8. APPENDIX A

For a surface with diffuse reflectance, one needs to know the sky averaged emissivity, ε_A, of the atmosphere to calculate the reflected sky radiance. A simple relation between ε_A and τ_0 (the zenith transmission) can be derived assuming the reflecting surface is horizontal and sees 2π of the sky.

The average can be written

$$\varepsilon_A = \frac{1}{2\pi}\int_0^{\pi/2} 2*\pi*\sin\theta*(1-\tau_0^{\sec\theta})*d\theta\,, \tag{A1}$$

$$= \int_0^{2\pi}(1-\tau_0^{\sec\theta})\,\sin\theta\,d\theta. \tag{A2}$$

Let $x = \cos\theta = 1/\sec\theta$. Then

$$\varepsilon_A = -\int_1^0 (1-\tau_0^{1/x})\,dx\,, \tag{A3}$$

$$= 1 - \int_0^1 \tau_0^{1/x}\,dx\,. \tag{A4}$$

This expression is straightforward to numerically integrate. Figure A1 shows the results of the integration as well as an empirical fit to the data. The empirical fit is

$$1 = \varepsilon_A^{1.54} + \tau_o^{1.54}, \tag{A5}$$

or

$$\varepsilon_A = (1 - \tau_o^{1.54})^{1/1.54} . \tag{A6}$$

Here, note that $\tau_o = f_1 * \tau_1$.

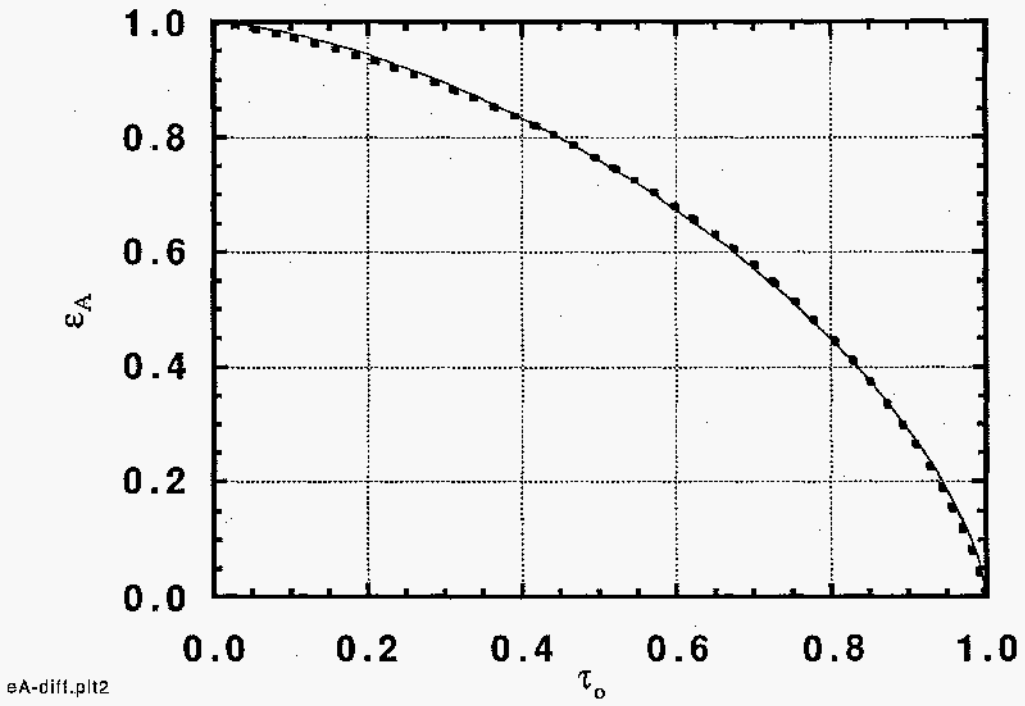

Figure A1. Comparison of numerical integration (short dashes) and empirical relation (thin line) for relation between sky averaged emissivity ε_A and zenith atmospheric transmission τ_o.